Adaptive DCS-SOMP for Localization Parameter Estimation in 5G Networks

Paulo Francisco da Conceição * and **Flávio Geraldo Coelho Rocha**

Department of Electrical, Mechanical and Computer Engineering, Federal University of Goiás, Goiânia 74605-010, Brazil; flaviogcr@ufg.br
* Correspondence: paulofrancisco@discente.ufg.br

Abstract: In this work, we model a 5G downlink channel using millimeter-wave (mmWave) and massive Multiple-Input Multiple-Output (mMIMO) technologies, considering the following localization parameters: Time of Arrival (TOA), Two-Dimensional Angle of Departure (2D-AoD), and Two-Dimensional Angle of Arrival (2D-AoA), both encompassing azimuth and elevation. Our research focuses on the precise estimation of these parameters within a three-dimensional (3D) environment, which is crucial in Industry 4.0 applications such as smart warehousing. In such scenarios, determining the device localization is paramount, as products must be handled with high precision. To achieve these precise estimations, we employ an adaptive approach built upon the Distributed Compressed Sensing—Subspace Orthogonal Matching Pursuit (DCS-SOMP) algorithm. We obtain better estimations using an adaptive approach that dynamically adapts the sensing matrix during each iteration, effectively constraining the search space. The results demonstrate that our approach outperforms the traditional method in terms of accuracy, speed to convergence, and memory use.

Keywords: 5G; compressed sensing; DCS-SOMP; parameter estimation

1. Introduction

Millimeter-wave (mmWave) and massive Multiple-Input Multiple-Output (mMIMO) technologies are some of the enablers for the future deployment of 5G and beyond 5G networks, constituting essential assets for realizing the full potential of disruptive 5G applications, especially those involving device localization, such as Industry 4.0, Unmanned Aerial Vehicles (UAVs), and Vehicle to Everything (V2X) communications. These technologies significantly enhance the accuracy of localization parameter estimation, such as the Time of Arrival (ToA), Angle of Departure (AoD), and Angle of Arrival (AoA) of signals.

Localization algorithms use localization parameters that can be estimated from the received signal using techniques such as Multiple Signal Classification (MUSIC) [1] and Compressed Sensing (CS) [2]. MUSIC-based methods analyze the cross-correlations among the received signals to identify the angles associated with their peaks in the power spectrum [3]. On the other hand, methods based on CS exploit the sparsity of signals, i.e., instead of acquiring the complete signal, CS enables accurate signal reconstruction using a few important components while the rest are negligible [2]. Among the CS-based methods, we highlight Distributed Compressed Sensing—Subspace Orthogonal Matching Pursuit (DCS-SOMP). DCS-SOMP combines the concept of CS with the Orthogonal Matching Pursuit (OMP) algorithm to handle sparse signals in a distributed environment or in systems with multiple antennas (e.g., mMIMO systems) [4].

In this work, we focus on the DCS-SOMP method, since it aligns more effectively with the sparse nature of mmWave signals. In [5,6], the DCS-SOMP method is applied to parameter estimation in a two-dimensional (2D) environment, providing only a coarse estimation of parameters which is followed by a refinement step using the Space-alternating Generalized Expectation-maximization (SAGE) method [7].

Our proposal has two novelties: first, our approach entails the dynamic adaptation of the sensing matrix, obtaining rapid and accurate parameter estimation through the DCS-SOMP method and second, we perform all parameter estimation within a three-dimensional (3D) environment. Our proposal relies on accurate channel modeling using two-dimensional AoD and AoA parameters coupled with Antennas's Uniform Circular Arrays (UCA).

The remainder of this article is organized as follows: in Section 2, a literature review is presented. Section 3 outlines the system model, focusing on the channel and received signal modeling. Section 4 elaborates on constructing the sensing matrix and applying the DCS-SOMP method, including the proposed modification for adaptive search in the sensing matrix. In Section 5, simulation results are presented and discussed. Finally, Section 6 concludes the article.

2. Related Works

Localization algorithms typically consist of two fundamental steps. First, the estimation of localization parameters extracted from the received signal. Second, using the acquired parameters from the first step, a localization method is employed to determine the position of the mobile station (MS) [5,8,9]. Regarding the first step, we highlight several aspects of the literature.

In [10], the authors estimate AoA and AoD using Sparse Bayes Tensor (SBT) from channel modeling using MIMO and mmWave. However, due to the use of a linear array of antennas, the proposed approach can only determine the azimuth of AoA and AoD and does not enable ToA estimation. In [8], the authors conduct indoor localization using channel modeling and ray tracing. They use two Uniform Linear Arrays (ULA), one perpendicular to the other, to extract the elevation angle. However, the method does not estimate AoD, thus preventing the use of algorithms dependent on this parameter.

In [5], the authors propose a comprehensive localization algorithm using MIMO, mmWave, and ULA. They employ the DCS-SOMP method for parameter estimation. Due to the linear antenna array, the method applies to a 2D environment. Additionally, the DCS-SOMP method provides only a coarse parameter estimate, demanding further fine-tuning using the SAGE method. In [11], the authors propose a 2D-AoA and 2D-AoD estimation using the MUSIC algorithm. The method utilizes a channel model with a rectangular Uniform Rectangular Array (URA). However, their proposal does not estimate ToA and only allows coarse angle estimation. Similarly to [5], the proposal in [11] requires fine-tuning techniques to provide accurate parameter estimations. In [12], the authors propose a technique named spatial spectrum fusion estimation and localization (SSFEAL) for performing 2D-AoA estimation using UCA in a MIMO mmWave channel.

In this work, we go beyond the related studies by proposing a joint estimation method of ToA, 2D-AoD, and 2D-AoA, enabling the use of these parameters in 3D localization algorithms in multipath environments. Furthermore, our proposed method accurately estimates the parameters without additional fine-tuning techniques. We employ a MIMO mmWave channel model with UCA to determine 2D-AoD and 2D-AoA, consistent with the works in [12,13]. Table 1 compares our proposal with others discussed in this section.

Table 1 demonstrates aspects of some related works and our proposal. Column 2 indicates the method used for parameter estimation. Column 3 displays the antenna array, while columns 4 to 6 specify whether the method estimates ToA, 2D-AoD, and 2D-AoA parameters, respectively. Our proposal presents the advantage of estimating all considered localization parameters (ToA, 2D-AoD, and 2D-AoA), while other methods estimate only some of them, or consider only two-dimensional (2D) environments. Additionally, our proposal utilizes the DCS-SOMP itself to achieve high accuracy, while other methods rely on extra algorithms for a refinement step. Although estimating five parameters increases the number of elements in the sensing matrix, our adaptive approach reduces execution time and yields more accurate results.

Table 1. Related work overview.

Article	Method	Array	ToA	2D-AoD	2D-AoA
[5]	DCS-SOMP	ULA	✓	×	×
[8]	MUSIC	ULA	✓	×	✓
[10]	SBT	ULA	×	×	×
[11]	MUSIC	URA	×	✓	✓
[12]	SSFEAL	UCA	×	×	✓
Our Proposal	Adaptive DCS-SOMP	UCA	✓	✓	✓

3. System Model

As outlined in the 3rd Generation Partnership Project (3GPP) guidelines released in the TR 38.901 V17.0.0 [14], we analyze a MIMO system with N_t transmitter antennas at the base station (BS) and N_r receiver antennas at the MS. This system operates at carrier frequency f_c and with bandwidth B. Similarly to [5], we consider the BS to send G signals to the receiver, where the g-th signal is composed of M_t symbols. Furthermore, we consider an indoor environment where there are L paths for the signals being transmitted from a single BS to the MS, such paths can be classified as Line of Sight (LoS) and single-bounce Non-Line of Sight (NLoS) paths. Multiple-bounce paths are not taken into account due to their limited reception strength at mmWave frequencies [15]. Additionally, we assume perfect clock synchronization, as in [16], enabling accurate ToA estimation.

Figure 1 illustrates a typical Industry 4.0 scenario in a smart warehouse where a forklift moves products from the conveyor belt to the shelves. In such a scenario, the localization and tracking of the forklift can be achieved using geometry-based methods, which rely on accurate estimation of localization parameters [5,17].
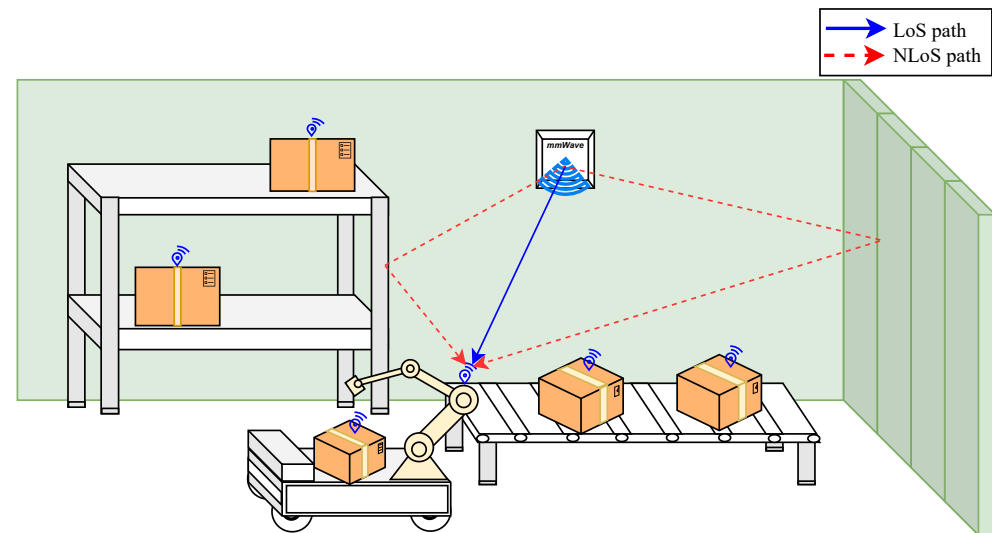
Figure 1. Indoor Localization Scenario with LoS and NLoS Paths: in a smart warehouse, a forklift is connected to a mmWave 5G network for product transport.

As in [14], we assume the channel's dependency on the response vector. Thus, for the n-th subcarrier (where $n = 0, ..., N - 1$), the channel matrix **H** can be represented as follows:

$$\mathbf{H}[n] = \sum_{l=1}^{L} \rho_l h_l e^{\frac{-j2\pi(n-1)\tau_l}{NT_s}} \sqrt{N_t} \mathbf{a}_t^H(\phi_l^{az}, \phi_l^{el}) \sqrt{N_r} \mathbf{a}_r(\theta_l^{az}, \theta_l^{el}),$$

(1)

where, for the l-th path, ρ_l represents the pathloss, h_l stands for the complex channel gain, τ_l is the ToA, ϕ_l^{az} is the azimuth AoD, ϕ_l^{el} is the elevation AoD, θ_l^{az} is the azimuth AoA, θ_l^{el} is the elevation AoA, and $T_s = 1/B$ denotes the sampling period. In order to take into

account 2D-AoD, i.e., $(\phi_l^{az}, \phi_l^{el})$ and 2D-AoA, i.e., $(\theta_l^{az}, \theta_l^{el})$, we employ a Uniform Circular Array (UCA) as in [13], thus we define the response vectors $\mathbf{a}_t$ and $\mathbf{a}_r$, as follows:

$$\mathbf{a}_t(\phi_l^{az}, \phi_l^{el}) = \left[1, e^{j\frac{2\pi}{\lambda}rsin(\phi_l^{el})cos(\phi_l^{az}-sin(1))}, \ldots, e^{j\frac{2\pi}{\lambda}rsin(\phi_l^{el})cos(\phi_l^{az}-sin(N_t-1))}\right], \tag{2}$$

$$\mathbf{a}_r(\theta_l^{az}, \theta_l^{el}) = \left[1, e^{j\frac{2\pi}{\lambda}rsin(\theta_l^{el})cos(\theta_l^{az}-sin(1))}, \ldots, e^{j\frac{2\pi}{\lambda}rsin(\theta_l^{el})cos(\theta_l^{az}-sin(N_r-1))}\right], \tag{3}$$

where λ is the wavelength, and r is the radius of the UCA. When a massive antenna array is used, as described in [13], the radius can be defined as $r = (N_t - 1)\frac{\lambda/2}{2\pi}$ for $\mathbf{a}_t(\phi_l^{az}, \phi_l^{el})$, and as $r = (N_r - 1)\frac{\lambda/2}{2\pi}$ for $\mathbf{a}_r(\theta_l^{az}, \theta_l^{el})$.

Finally, the received signal for subcarrier n and transmission g can be expressed as follows:

$$\boldsymbol{y}^{(g)}[n] = \mathbf{H}[n]\boldsymbol{x}^{(g)}[n] + \boldsymbol{w}[n], \tag{4}$$

where $\boldsymbol{x}^{(g)}$ represents the signal with the transmitted data symbols, and $\boldsymbol{w}$ denotes a Gaussian noise vector with a zero mean and variance σ^2.

4. Proposed Method

For ease of understanding, we divide our proposal into two stages: (1) sensing matrix construction and (2) 3D parameter estimation using the DCS-SOMP algorithm.

4.1. Sensing Matrix Construction

According to [14], the azimuth angle belongs to the interval $[0, 2\pi]$ and the elevation angle belongs to the interval $[0, \pi]$. Therefore, we have q_{az} candidates for azimuth angles uniformly spaced within the interval $[0, 2\pi]$, and q_{el} candidates for elevation angles uniformly spaced within the interval $[0, \pi]$. We define $\tilde{\boldsymbol{\phi}}^{(0)} = [\tilde{\phi}_1^{(0)}, \ldots, \tilde{\phi}_{q_{az}}^{(0)}]$, $\dot{\boldsymbol{\phi}}^{(0)} = [\dot{\phi}_1^{(0)}, \ldots, \dot{\phi}_{q_{el}}^{(0)}]$ as candidates for AoD azimuth and elevation, respectively, and $\tilde{\boldsymbol{\theta}}^{(0)} = [\tilde{\theta}_1^{(0)}, \ldots, \tilde{\theta}_{q_{az}}^{(0)}]$, $\dot{\boldsymbol{\theta}}^{(0)} = [\dot{\theta}_1^{(0)}, \ldots, \dot{\theta}_{q_{el}}^{(0)}]$ as candidates for AoA azimuth and elevation, respectively. We introduce the matrix $\mathbf{U}_t^{(0)}$ of dimensions $N_t \times q_{az}q_{el}$ containing the response vectors for each possible combination of azimuth and elevation for AoD:

$$\mathbf{U}_t^{(0)} = [\mathbf{a}_t(\tilde{\boldsymbol{\phi}}^{(0)}, \dot{\boldsymbol{\phi}}^0)]. \tag{5}$$

Similarly, we create the matrix $\mathbf{U}_r^{(0)}$ of dimensions $N_r \times q_{az}q_{el}$ containing the response vectors for each possible combination of azimuth and elevation for AoA:

$$\mathbf{U}_r^{(0)} = [\mathbf{a}_t(\tilde{\boldsymbol{\theta}}^{(0)}, \dot{\boldsymbol{\theta}}^{(0)})]. \tag{6}$$

Finally, we obtain the sensing matrix $\boldsymbol{\omega}^{(0)}$ as follows:

$$\boldsymbol{\omega}^{(0)}[n] = (\mathbf{U}_t^{(0)}\mathbf{x}^{(g)}[n])^T \otimes \mathbf{U}_r^{(0)}, \tag{7}$$

where $\mathbf{x}^{(g)}$ represents the transmitted data and $\otimes$ denotes the Kronecker product. The sensing matrix $\boldsymbol{\omega}$ has dimensions of $(N_t M_t) \times (q_{az}M_t)^2$. As a result, the number of elements in $\boldsymbol{\omega}$ is directly related and highly sensitive to the values of q_{az} and q_{el}.

In Section 5, we have demonstrated that increasing the number of candidates (q_{az}, q_{el}) for DCS-SOMP is crucial to achieving accurate estimations of 2D-AoD and 2D-AoA. However, an increased number of candidates also leads to increased memory usage, as shown in Figure 2. Our proposed modification to DCS-SOMP introduces an adaptive search approach, dynamically adjusting the sensing matrix during each iteration, as detailed in Section 4.3, to address this issue.
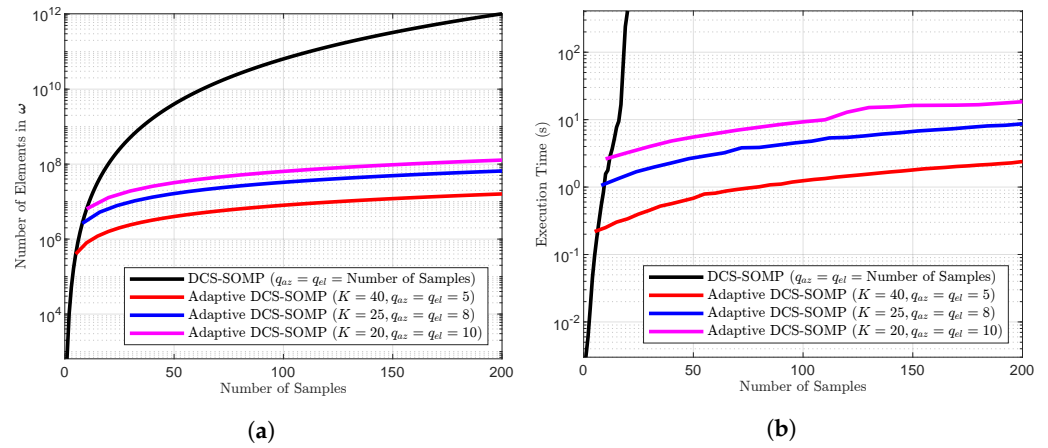
Figure 2. Comparison between DCS-SOMP and Adaptive DCS-SOMP: (**a**) Variation in Sensing Matrix Size (Number of Elements) and (**b**) Execution Time, both regarding the number of samples.

4.2. DCS-SOMP Approach for 3D Parameter Estimation

The DCS-SOMP method determines the index $\tilde{h}_l$ of the maximum correlation between (4) and (7). Therefore, for the *l*-th path, $\tilde{h}_l$ is defined as follows:

$$\tilde{h}_l = \underset{m=1,\ldots,(q_{az}q_{el})^2}{\arg\max} \sum_{n=1}^{N} \frac{|\boldsymbol{\omega}_m^{\mathrm{H}}[n]\mathbf{R}_l[n]|}{\|\boldsymbol{\omega}_m[n]\|_2}, \tag{8}$$

where $\mathbf{R}_l$ represents the received signal's residue and *m* represents each column in $\boldsymbol{\omega}$. $\mathbf{R}_l = \boldsymbol{y}$ when $l = 1$.

The index $\tilde{h}_l$ is converted into a combination of $(\phi_l^{az}, \phi_l^{el})$ and $(\theta_l^{az}, \theta_l^{el})$. The 2D-AoD $(\phi_l^{az}, \phi_l^{el})$ is determined as follows:

$$I_\phi^l = \frac{\tilde{h}_l}{q_{az}q_{el}}, \quad \iota_l^{az} = \left\lfloor \frac{I_\phi^l}{q_{az}} \right\rfloor, \quad \iota_l^{el} = I_\phi^l \bmod q_{el}, \tag{9}$$

$$\phi_l^{az} = \tilde{\boldsymbol{\phi}}_{\iota_l^{az}}^{(0)}, \quad \phi_l^{el} = \dot{\boldsymbol{\phi}}_{\iota_l^{el}}^{(0)}. \tag{10}$$

Similarly, the 2D-AoA $(\theta_l^{az}, \theta_l^{el})$ is determined as follows:

$$I_\theta^l = \tilde{h}_l - I_\phi^l q_{az}q_{el}, \quad \gamma_l^{az} = \left\lfloor \frac{I_\theta^l}{q_{az}} \right\rfloor, \quad \gamma_l^{el} = I_\theta^l \bmod q_{el}, \tag{11}$$

$$\theta_l^{az} = \tilde{\boldsymbol{\theta}}_{\gamma_l^{az}}^{(0)}, \quad \theta_l^{el} = \dot{\boldsymbol{\theta}}_{\gamma_l^{el}}^{(0)}. \tag{12}$$

Finally, the DCS-SOMP method updates the residual for the *n*-th subcarrier as follows:

$$\beta_l[n] = \frac{\boldsymbol{\omega}_{\tilde{h}_l}^{\mathrm{H}}[n]\mathbf{R}_l[n]}{\|\boldsymbol{\omega}_{\tilde{h}_l}[n]\|_2^2}, \tag{13}$$

$$\mathbf{R}_{l+1}[n] = \mathbf{R}_l[n] - \beta_l[n]\boldsymbol{\omega}_{\tilde{h}_l}[n]. \tag{14}$$

Similar to [5], the estimation of ToA provides a maximum distance of NT_sc (m). Therefore, ToA can be estimated as follows:

$$\text{distance} = \frac{1}{N}\left[\sum_{n=1}^{N} \beta_l[n]\right] NT_s \frac{c}{2\pi}, \tag{15}$$

$$\tau_l = \begin{cases} \text{distance}/c \text{ , if distance } \geq 0 \\ (\text{distance} + NT_sc)/c \text{ , if distance} < 0, \end{cases} \tag{16}$$

where *c* is the speed of light.

4.3. Adaptive Search in DCS-SOMP Approach for 3D Parameter Estimation

We introduce an adaptive approach to enhance the parameters estimated in the two aforementioned stages: (1) sensing matrix construction and (2) application of the DCS-SOMP approach for 3D parameter estimation. Our method dynamically adapts the search space for each angle to be estimated, i.e., 2D-AoD and 2D-AoA. To illustrate how dynamic adaptation is performed, Figure 3 demonstrates the improvements made in each iteration using our adaptive approach for the azimuth AoD angle. In summary, in iteration *k*, the search interval ($\tilde{\boldsymbol{\phi}}^{(k)}$) is dynamically adapted using the index (ι_l^{az}) of the previous search interval ($\tilde{\boldsymbol{\phi}}^{(k-1)}$). New parameters are estimated in each iteration. The process continues until a predetermined number of iterations (*K*) is reached or a pre-established threshold (ϱ) is exceeded.
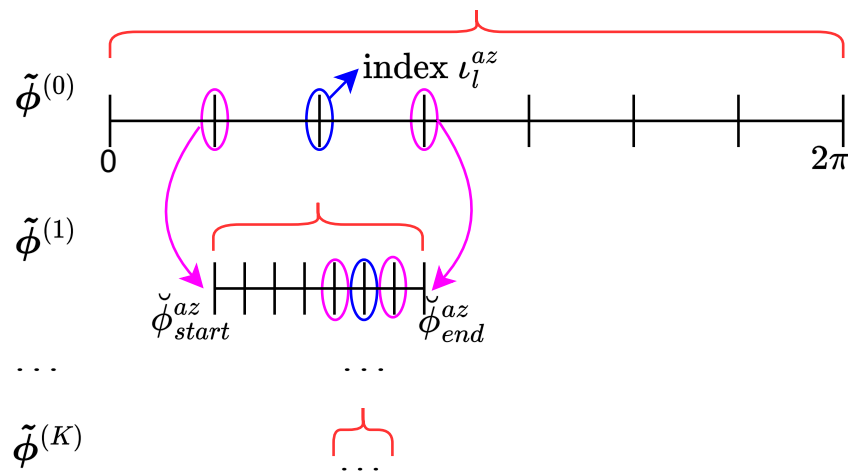
Figure 3. Adaptive Procedure for Selecting Eligible Candidates for Azimuth AoD.

We adaptively calculate the candidates for AoD azimuth angle ($\tilde{\boldsymbol{\phi}}^{(k)}$) with q_{az} values that are uniformly spaced within a new interval $[\check{\phi}_{start}^{az}, \check{\phi}_{end}^{az}]$, where

$$\check{\phi}_{start}^{az} = \begin{cases} \tilde{\boldsymbol{\phi}}_{\iota_l^{az}-1}^{(k-1)}, & \text{if } \iota_l^{az} > 1 \\ 0, & \text{if } \iota_l^{az} = 1 \end{cases} \quad \text{and} \quad \check{\phi}_{end}^{az} = \begin{cases} \tilde{\boldsymbol{\phi}}_{\iota_l^{az}+1}^{(k-1)}, & \text{if } \iota_l^{az} < q_{az} \\ q_{az}, & \text{if } \iota_l^{az} = q_{az} \end{cases}. \tag{17}$$

Similarly, we adaptively calculate the candidates for AoD elevation angle ($\dot{\boldsymbol{\phi}}^{(k)}$) with q_{el} values that are uniformly spaced within a new interval $[\check{\phi}_{start}^{el}, \check{\phi}_{end}^{el}]$, where

$$\check{\phi}_{start}^{el} = \begin{cases} \dot{\boldsymbol{\phi}}_{\iota_l^{el}-1}^{(k-1)}, & \text{if } \iota_l^{el} > 1 \\ 0, & \text{if } \iota_l^{el} = 1 \end{cases} \quad \text{and} \quad \check{\phi}_{end}^{el} = \begin{cases} \dot{\boldsymbol{\phi}}_{\iota_l^{el}+1}^{(k-1)}, & \text{if } \iota_l^{el} < q_{el} \\ q_{el}, & \text{if } \iota_l^{el} = q_{el} \end{cases}. \tag{18}$$

For the AoA azimuth angle, we adaptively calculate the candidates ($\tilde{\boldsymbol{\theta}}^{(k)}$) with q_{az} values that are uniformly spaced within a new interval $[\check{\theta}_{start}^{az}, \check{\theta}_{end}^{az}]$, where

$$\check{\theta}_{start}^{az} = \begin{cases} \tilde{\boldsymbol{\theta}}_{\gamma_l^{az}-1}^{(k-1)}, & \text{if } \gamma_l^{az} > 1 \\ 0, & \text{if } \gamma_l^{az} = 1 \end{cases} \quad \text{and} \quad \check{\theta}_{end}^{az} = \begin{cases} \tilde{\boldsymbol{\theta}}_{\gamma_l^{az}+1}^{(k-1)}, & \text{if } \gamma_l^{az} < q_{az} \\ q_{az}, & \text{if } \gamma_l^{az} = q_{az} \end{cases}. \tag{19}$$

Similarly, we adaptively calculate the candidates for AoA elevation angle $(\dot{\boldsymbol{\theta}}^{(k)})$ with q_{el} values that are uniformly spaced within a new interval $[\breve{\theta}_{start}^{el}, \breve{\theta}_{end}^{el}]$, where

$$
\breve{\theta}_{start}^{el} = \begin{cases} \dot{\boldsymbol{\theta}}_{\gamma_l^{el}-1}^{(k-1)}, & \text{if } \gamma_l^{el} > 1 \\ 0, & \text{if } \gamma_l^{el} = 1 \end{cases} \quad \text{and} \quad \breve{\theta}_{end}^{el} = \begin{cases} \dot{\boldsymbol{\theta}}_{\gamma_l^{el}+1}^{(k-1)}, & \text{if } \gamma_l^{el} < q_{el} \\ q_{el}, & \text{if } \gamma_l^{el} = q_{el} \end{cases}. \tag{20}
$$

Thus, using $\tilde{\boldsymbol{\phi}}^{(k)}$, $\dot{\boldsymbol{\phi}}^{(k)}$, $\tilde{\boldsymbol{\theta}}^{(k)}$, and $\dot{\boldsymbol{\theta}}^{(k)}$ we determine the new sensing matrix as follows:

$$
\mathbf{U}_t^{(k)} = [\mathbf{a}_t(\tilde{\boldsymbol{\phi}}^{(k)}, \dot{\boldsymbol{\phi}}^k)], \tag{21}
$$

$$
\mathbf{U}_r^{(k)} = [\mathbf{a}_t(\tilde{\boldsymbol{\theta}}^{(k)}, \dot{\boldsymbol{\theta}}^{(k)})], \tag{22}
$$

$$
\boldsymbol{\omega}^{(k)}[n] = (\mathbf{U}_t^{(k)} \mathbf{x}^{(g)}[n])^T \otimes \mathbf{U}_r^{(k)}. \tag{23}
$$

Using $\mathbf{R}_l$ and $\boldsymbol{\omega}^{(k)}$, we determine new values for $(\phi_l^{az}, \phi_l^{el})$, $(\theta_l^{az}, \theta_l^{el})$, and τ_l^{el} from (10), (12), and (16), respectively, which initiates a new iteration. Although the adaptive step enhances the sensing matrix for 2D-AoD and 2D-AoA estimation, it also yields improvements in ToA estimation. The continual improvement of the maximum correlation with each iteration in the adaptive process positively impacts the ToA estimation accuracy.

Therefore, our adaptive approach involves using a smaller number for q_{az} and q_{el}, enabling us to achieve a high number of samples in the overall search space while consuming less memory. This is due to the reduced size of the matrix $\boldsymbol{\omega}$ in terms of its total number of elements. Additionally, our approach requires less time than the simple method while maintaining greater accuracy.

Figure 2a,b clearly demonstrates that when using the DCS-SOMP method, a small sample space is accommodated, should memory space or execution time be constrained. The simulations reveal that when using over 18 samples in the sensing matrix, the DCS-SOMP method becomes impractical in terms of execution time and memory. On the other hand, the adaptive method consumes less memory, exhibits shorter execution times, and is capable of accommodating larger sample spaces. Furthermore, the sample space accommodated by the adaptive method consistently remains close to the actual value, enhancing its precision. We calculate the number of elements $(q_{\boldsymbol{\omega}})$ in $\boldsymbol{\omega}$ using the formula: $q_{\boldsymbol{\omega}} = ((N_t M_t)(q_{az}q_{el})^2)K$, where $K = 1$ for DCS-SOMP. To generate Figure 2a, we arbitrarily set the number of antennas at the transmitter to $N_t = 32$ and the number of transmitted symbols to $M_t = 20$, similar results were obtained with other values.

Algorithm 1 outlines our proposal. The adaptive search step is called at line 17. Algorithm 2 provides a summary of the adaptive search step.

Algorithm 1 Modified DCS-SOMP

Input: y, $\omega^{(0)}$, $\tilde{\boldsymbol{\phi}}^{(0)}$, $\dot{\boldsymbol{\phi}}^{(0)}$, $\tilde{\boldsymbol{\theta}}^{(0)}$, $\dot{\boldsymbol{\theta}}^{(0)}$, q_{az}, q_{el}, K, L, N
Output: ϕ_l^{az}, ϕ_l^{el}, θ_l^{az}, θ_l^{el}, τ_l
1: $\mathbf{R}_1 \leftarrow y$
2: **for** $l \leftarrow 1$ to L **do**
3:      $\tilde{h}_l \leftarrow -1$
4:      $\max_{corr} \leftarrow -1$ ▷ *Maximum Correlation*
5:      **for** $m \leftarrow 1$ to $(q_{az}q_{el})^2$ **do**
6:         $\text{corr} \leftarrow 0$
7:         **for** $n \leftarrow 1$ to N **do**
8:            $\text{corr} \leftarrow \text{corr} + \frac{[\omega_m^{(0)}[n]]^T \mathbf{R}_l[n]}{\|\omega_m^{(0)}[n]\|_2}$
9:         **end for**
10:        **if** $\text{corr} > \max_{corr}$ **then**
11:           $\tilde{h}_l \leftarrow m$
12:        **end if**
13:      **end for**
14:      Determine ι_l^{az}, ι_l^{el}, γ_l^{az} and γ_l^{el} from (9) and (11)
15:      Determine $(\phi_l^{az}, \phi_l^{el})$ from (10)
16:      Determine $(\theta_l^{az}, \theta_l^{el})$ from (12)
17:      Using $[\mathbf{R}_l, \iota_l^{az}, \iota_l^{el}, \gamma_l^{az}, \gamma_l^{el}, \tilde{\boldsymbol{\phi}}^{(0)}, \dot{\boldsymbol{\phi}}^{(0)}, \tilde{\boldsymbol{\theta}}^{(0)}, K, N, q_{az}, q_{el}]$ as input, fine-tune $[\phi_l^{az}, \phi_l^{el}, \theta_l^{az}, \theta_l^{el}, \tau_l]$ using Algorithm 2
18:      **for** $n \leftarrow 1$ to N **do**
19:         Determine $\beta_l[n]$ from (13)
20:         Determine $\mathbf{R}_{l+1}[n]$ from (14)
21:      **end for**
22:      Determine τ_l from (16)   ▷ *Execute solely if the adaptive step is not called*
23: **end for**

Algorithm 2 Adaptive Search

Input: $\mathbf{R}_l$, ι_l^{az}, ι_l^{el}, γ_l^{az}, γ_l^{el}, $\tilde{\boldsymbol{\phi}}^{(0)}$, $\dot{\boldsymbol{\phi}}^{(0)}$, $\tilde{\boldsymbol{\theta}}^{(0)}$, K, N, q_{az}, q_{el}
Output: ϕ_l^{az}, ϕ_l^{el}, θ_l^{az}, θ_l^{el}, τ_l
1: **for** $k \leftarrow 1$ to K **do**
2:      Determine $[\breve{\phi}_{start}^{az}, \breve{\phi}_{end}^{az}]$ from (17)
3:      Determine $[\breve{\phi}_{start}^{el}, \breve{\phi}_{end}^{el}]$ from (18)
4:      Determine $[\breve{\theta}_{start}^{az}, \breve{\theta}_{end}^{az}]$ from (19)
5:      Determine $[\breve{\theta}_{start}^{el}, \breve{\theta}_{end}^{el}]$ from (20)
6:      $\tilde{\boldsymbol{\phi}}^{(k)} \leftarrow [\breve{\phi}_{start}^{az}, \dots, \breve{\phi}_{end}^{az}]$ ▷ q_{az} *values uniformly spaced*
7:      $\dot{\boldsymbol{\phi}}^{(k)} \leftarrow [\breve{\phi}_{start}^{el}, \dots, \breve{\phi}_{end}^{el}]$ ▷ q_{el} *values uniformly spaced*
8:      $\tilde{\boldsymbol{\theta}}^{(k)} \leftarrow [\breve{\theta}_{start}^{az}, \dots, \breve{\theta}_{end}^{az}]$ ▷ q_{az} *values uniformly spaced*
9:      $\dot{\boldsymbol{\theta}}^{(k)} \leftarrow [\breve{\theta}_{start}^{el}, \dots, \breve{\theta}_{end}^{el}]$ ▷ q_{el} *values uniformly spaced*
10:      **for** $n \leftarrow 1$ to N **do**
11:         Determine $\omega^{(k)}[n]$ from (23)
12:      **end for**
13:      $\tilde{h}_l \leftarrow -1$
14:      $\max_{corr} \leftarrow -1$ ▷ *Maximum Correlation*
15:      **for** $m \leftarrow 1$ to $(q_{az}q_{el})^2$ **do**
16:         $\text{corr} \leftarrow 0$
17:         **for** $n \leftarrow 1$ to N **do**
18:            $\text{corr} \leftarrow \text{corr} + \frac{[\omega_m^{(k)}[n]]^T \mathbf{R}_l[n]}{\|\omega_m^{(k)}[n]\|_2}$
19:         **end for**
20:         **if** $\text{corr} > \max_{corr}$ **then**
21:           $\tilde{h}_l \leftarrow m$
22:         **end if**
23:      **end for**
24:      Determine ι_l^{az}, ι_l^{el}, γ_l^{az} and γ_l^{el} from (9) and (11)
25:      Determine $(\phi_l^{az}, \phi_l^{el})$ from (10)
26:      Determine $(\theta_l^{az}, \theta_l^{el})$ from (12)
27:      **for** $n \leftarrow 1$ to N **do**
28:         Determine $\beta_l[n]$ from (13)
29:      **end for**
30:   Determine τ_l from (16)
31: **end for**

5. Results

In this article, we conducted simulations using MATLAB® software version R2012b (used under an academic license) installed in a computer running Windows 11 as the operating system and with the following hardware configurations: 2.5 GHz Intel Core i5-10300H processor, 16 GB RAM, and NVIDIA GTX 1650 as the dedicated video card.

We selected arbitrary actual values for two paths as described in Table 2. We set $q_{az} = 18$ and $q_{el} = 18$ when not using the adaptive search, i.e., DCS-SOMP, as this is the maximum value our simulator could process. When using the adaptive search, we set $q_{az} = 6$ and $q_{el} = 6$. Additionally, we defined the parameters as follows: $f_c = 28$ GHz, $B = 100$ MHz, $N_t = 64$, $N_r = 64$, $N = 10$, and $M_t = 20$. To establish a maximum number of iterations, we determined the difference between the estimated value in iteration k and the estimated value in iteration $k - 1$, and as long as this difference is greater than the threshold ($\varrho = 10^{-6}$), the next iteration will be performed.

Table 2. Actual Values Used in Simulations.

Path	ϕ^{az} (rad)	ϕ^{el} (rad)	θ^{az} (rad)	θ^{el} (rad)	τ (us)
1	1.33	0.45	3.50	0.90	0.0615
2	2.80	1.15	5.20	1.45	0.0767

Figures 4a–6 display the comparison between DCS-SOMP and adaptive DCS-SOMP for 2D-AoD, 2D-AoA, and ToA. The results correspond to a random run for Path 1. It's evident that, for all cases, the adaptive DCS-SOMP significantly enhances the estimation of the respective angle as early as the second iteration, gradually converging towards the actual value with each subsequent iteration.

(**a**) (**b**)
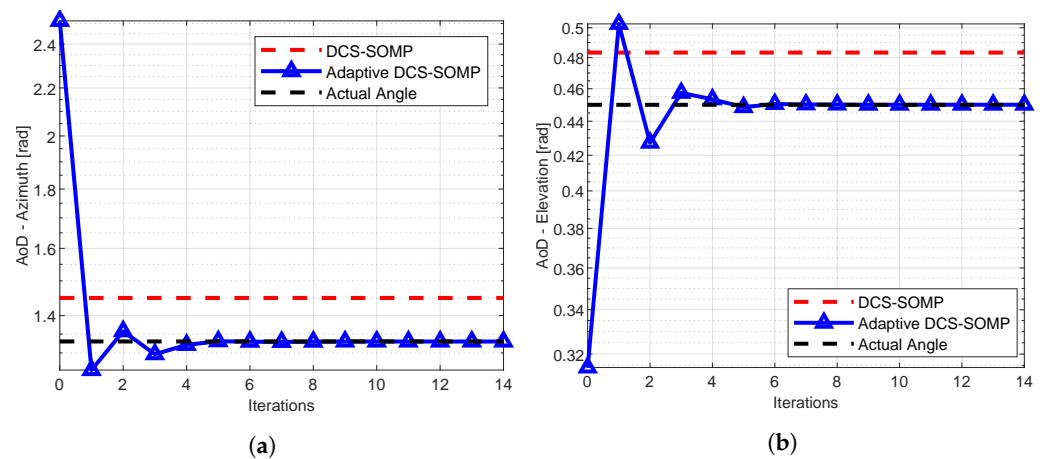
Figure 4. Comparison of (**a**) Azimuth AoD estimation and (**b**) Elevation AoD estimation results using DCS-SOMP and adaptive DCS-SOMP. The outcomes pertain to Path 1. In the DCS-SOMP case, q_{az} and q_{el} are both set to 18, whereas in the adaptive DCS-SOMP scenario, q_{az} and q_{el} are both set to 6.

We analyzed the complexity of the methods in terms of execution time and number of mathematical operations. Following the analysis provided in [18,19], the complexity of the SOMP algorithm is $O(LN_t q_c)$, where $q_c = q_{az} q_{el}$ denotes all possible combinations for the candidates for azimuth (q_{az}) and elevation angles (q_{el}). In the DCS-SOMP algorithm, we perform the Kronecker product (tensor product for matrices) to estimate 2D-AoD and 2D-AoA parameters, resulting in $O(LN_t(q_c)^2)$. In our adaptive DCS-SOMP approach, we fix the number of candidates and we update the values for the candidates at each iteration. Thus, the complexity of the adaptive DCS-SOMP is $O(LN_t q_c q_{it})$, where q_{it} is the number of

iterations. The main mathematical operations are due to (7) and (8). We determine the total number of mathematical operations, q_{op}, as follows:
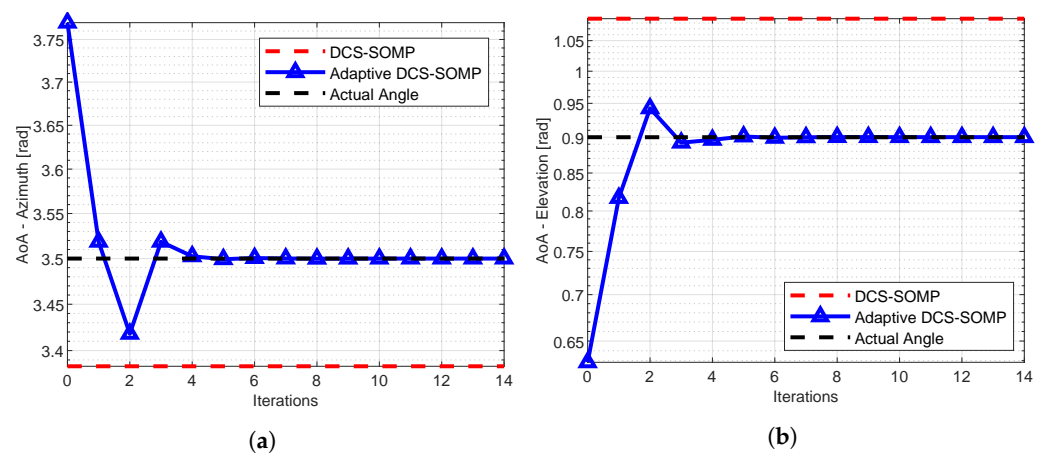
$$q_{op} = (q_{op}^w + q_{op}^h)(q_{it}L + 1), \tag{24}$$

where q_{op}^w is the number of mathematical operations to construct the sensing matrix, (7), determined as follows:

$$q_{op}^w = N(q_c M_t N_t + q_c(M_t N_t - 1) + M_t N_t(q_c)^2), \tag{25}$$

and q_{op}^h is the number of mathematical operations to determine the max correlation, (8), determined as follows:

$$q_{op}^h = (2N_t M_t)N(q_c)^2. \tag{26}$$

Figure 5. Comparison of (**a**) Azimuth AoA estimation and (**b**) Elevation AoA estimation results using DCS-SOMP and adaptive DCS-SOMP. The outcomes pertain to Path 1. In the DCS-SOMP case, q_{az} and q_{el} are both set to 18, whereas in the adaptive DCS-SOMP scenario, q_{az} and q_{el} are both set to 6.
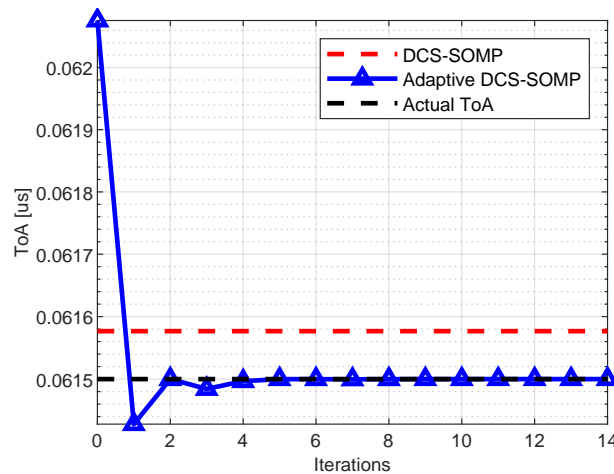
Figure 6. Comparison of ToA estimation results using DCS-SOMP and adaptive DCS-SOMP. The outcomes pertain to Path 1. In the DCS-SOMP case, q_{az} and q_{el} are both set to 18, whereas in the adaptive DCS-SOMP case, q_{az} and q_{el} are both set to 6.

Table 3 presents the execution times and the number of mathematical operations for each method. For the adaptive DCS-SOMP method, we utilized 14 iterations. These values represent the total duration required by the method to estimate all five parameters for both paths. Our observations indicate that the adaptive method is notably faster and involves fewer mathematical operations compared to the traditional method.

Table 3. Comparison between DCS-SOMP and Adaptive DCS-SOMP.

Method	Time (s)	Number of Mathematical Operations
DCS-SOMP	84.63	4.0393×10^9
Adaptive DCS-SOMP	0.88	1.4697×10^9

We used the Root Mean Square Error (RMSE) as the Key Performance Indicator (KPI) for our estimates. The RMSE ε is calculated as follows:

$$\varepsilon = \sqrt{\frac{1}{Q} \sum_{i=1}^{Q} |p_i - \hat{p}_i|^2}, \tag{27}$$

where Q is the number of runs, p_i is the actual value of the chosen parameter at the *i*-th run, and $\hat{p}_i$ is the estimated value of the chosen parameter at the *i*-th run.

Table 4 presents the RMSE for each parameter estimated, where $\varepsilon_{\phi^{az}}$, $\varepsilon_{\phi^{el}}$, $\varepsilon_{\theta^{az}}$, $\varepsilon_{\theta^{el}}$, and ε_τ represent the RMSE for azimuth AoD, elevation AoD, azimuth AoA, elevation AoA, and ToA, respectively. The RMSE was determined from 100 runs of each method, considering the average across all paths. The adaptive method exhibits higher precision compared to the non-adaptive method for all analyzed parameters.

Table 4. Comparison of RMSE between DCS-SOMP and adaptive DCS-SOMP.

Method	$\varepsilon_{\phi^{az}}$ (rad)	$\varepsilon_{\phi^{el}}$ (rad)	$\varepsilon_{\theta^{az}}$ (rad)	$\varepsilon_{\theta^{el}}$ (rad)	ε_τ (us)
DCS-SOMP	0.1334	0.0454	0.1087	0.2851	0.0109
Adaptive DCS-SOMP	0.0017	0.0005	0.0089	0.0256	0.0001

6. Conclusions

In this work, we addressed the problem of low performance presented by traditional DCS-SOMP approaches, which present convergence and precision to estimate parameters only at the cost of low performance. To achieve this, we proposed an adaptive DCS-SOMP method that dynamically calculates the sensing matrix, presenting high performance in precisely estimating localization parameters while keeping the algorithm simple and with fast convergence.

This modification transformed the DCS-SOMP method from solely a coarse estimator to a singular tool for precise parameter estimation. Even in a 3D environment with five parameters to be estimated and multiple paths to be detected, the adaptive DCS-SOMP method exhibited substantial improvements in both accuracy and speed compared to the DCS-SOMP approach. Further enhancements to the adaptive DCS-SOMP could be explored, such as refining the way the residue was updated, potentially enabling improved separation of paths. Furthermore, we plan to explore alternative antenna arrays, including 2D configurations, to enhance beam-forming capabilities in mmWave scenarios within 5G and B5G networks.

Author Contributions: All authors (P.F.d.C. and F.G.C.R.) contributed equally to this article. All authors have read and agreed to the published version of the manuscript.

Conflicts of Interest: The authors declare no conflict of interest.

References

1. Schmidt, R. Multiple Emitter Location and Signal Parameter Estimation. *IEEE Trans. Antennas Propag.* **1986**, *34*, 276–280. [CrossRef]
2. Donoho, D. Compressed Sensing. *IEEE Trans. Inf. Theory* **2006**, *52*, 1289–1306. [CrossRef]
3. Liu, G.; Chen, H.; Sun, X.; Qiu, R.C. Modified MUSIC Algorithm for DOA Estimation with Nyström Approximation. *IEEE Sens. J.* **2016**, *16*, 4673–4674. [CrossRef]
4. Duarte, M.; Sarvotham, S.; Baron, D.; Wakin, M.; Baraniuk, R. Distributed Compressed Sensing of Jointly Sparse Signals. In Proceedings of the Conference Record of the Thirty-Ninth Asilomar Conference on Signals, Systems and Computers, Pacific Grove, CA, USA, 30 October–2 November 2005; pp. 1537–1541. [CrossRef]
5. Shahmansoori, A.; Garcia, G.E.; Destino, G.; Seco-Granados, G.; Wymeersch, H. Position and Orientation Estimation Through Millimeter-Wave MIMO in 5G Systems. *IEEE Trans. Wirel. Commun.* **2018**, *17*, 1822–1835. [CrossRef]
6. Fascista, A.; Coluccia, A.; Wymeersch, H.; Seco-Granados, G. Low-Complexity Accurate Mmwave Positioning for Single-Antenna Users Based on Angle-of-Departure and Adaptive Beamforming. In Proceedings of the ICASSP 2020—2020 IEEE International Conference on Acoustics, Speech and Signal Processing (ICASSP), Barcelona, Spain, 4–8 May 2020; pp. 4866–4870.
7. Fessler, J.; Hero, A. Space-alternating Generalized Expectation-maximization Algorithm. *IEEE Trans. Signal Process.* **1994**, *42*, 2664–2677. [CrossRef]
8. Wang, Y.; Zhao, K.; Zheng, Z. An Improved 3D Indoor Positioning Study with Ray Tracing Modeling for 6G Systems. *Mob. Netw. Appl.* **2023**. [CrossRef]
9. Chen, H.; Kim, H.; Ammous, M.; Seco-Granados, G.; Alexandropoulos, G.C.; Valaee, S.; Wymeersch, H. RISs and Sidelink Communications in Smart Cities: The Key to Seamless Localization and Sensing. *IEEE Commun. Mag.* **2023**, *61*, 140–146. [CrossRef]
10. Luo, K.; Zhou, X.; Wang, B.; Huang, J.; Liu, H. Sparse Bayes Tensor and DOA Tracking Inspired Channel Estimation for V2X Millimeter Wave Massive MIMO System. *Sensors* **2021**, *21*, 4021. [CrossRef]
11. Grishin, I.; Fokin, G.; Sevidov, V.; Okuneva, D. Analysis of the Spatial Smoothing Influence on the Perfomance of 2D-MUSIC for Ultra-Dense Networks. In Proceedings of the 2023 Wave Electronics and its Application in Information and Telecommunication Systems (WECONF), St. Petersburg, Russia, 30 May–3 June 2022; pp. 1–6. [CrossRef]
12. He, D.; Chen, X.; Pei, L.; Zhu, F.; Jiang, L.; Yu, W. Multi-BS Spatial Spectrum Fusion for 2-D DOA Estimation and Localization Using UCA in Massive MIMO System. *IEEE Trans. Instrum. Meas.* **2021**, *70*, 5500213. [CrossRef]
13. Tan, W.; Ma, S. Antenna Array Topologies for mmWave Massive MIMO Systems: Spectral Efficiency Analysis. *IEEE Trans. Veh. Technol.* **2022**, *71*, 12901–12915. [CrossRef]
14. 3GPP. Study on Channel Model for Frequencies from 0.5 to 100 GHz (3GPP TR 38.901 Version 17.0.0 Release 17). Technical Specification (TS) 38.901, 3rd Generation Partnership Project (3GPP), Version 17.0.0. 2022. Available online: https://portal.etsi.org/webapp/workprogram/Report_WorkItem.asp?WKI_ID=65119 (accessed on 10 August 2023).
15. Kakkavas, A.; Wymeersch, H.; Seco-Granados, G.; García, M.H.C.; Stirling-Gallacher, R.A.; Nossek, J.A. Power Allocation and Parameter Estimation for Multipath-Based 5G Positioning. *IEEE Trans. Wirel. Commun.* **2021**, *20*, 7302–7316. [CrossRef]
16. Quan, X.; Niu, K.; Dong, C.; Yu, Y. Joint Approximate Maximum Likelihood Localization Algorithm in 5G New Radio Systems. In Proceedings of the 2020 IEEE 31st Annual International Symposium on Personal, Indoor and Mobile Radio Communications, London, UK, 31 August–3 September 2020; pp. 1–6. [CrossRef]
17. Sellami, A.; Nasraoui, L.; Najjar, L. Analysis of Localization Performance in mm-Wave 5G Network Under Channel Uncertainties. *IEEE Internet Things J.* **2023**, *10*, 6523–6524. [CrossRef]
18. Qi, C.; Wu, L. A hybrid compressed sensing algorithm for sparse channel estimation in MIMO OFDM systems. In Proceedings of the 2011 IEEE International Conference on Acoustics, Speech and Signal Processing (ICASSP), Prague, Czech Republic, 22–27 May 2011; pp. 3488–3491. [CrossRef]
19. Zhou, Y.; Tong, F.; Song, A.; Diamant, R. Exploiting Spatial–Temporal Joint Sparsity for Underwater Acoustic Multiple-Input–Multiple-Output Communications. *IEEE J. Ocean. Eng.* **2021**, *46*, 352–369. [CrossRef]